NEURAL REGENERATION RESEARCH
www.nrronline.org

Research Article

Ginsenoside Rb1 improves energy metabolism after spinal cord injury

Shan Wen[1, 2], Zhi-Ru Zou[2, 3], Shuai Cheng[1, 2], Hui Guo[1, 2], Heng-Shuo Hu[1, 2], Fan-Zhuo Zeng[1, 2], Xi-Fan Mei[1, 2, *]

https://doi.org/10.4103/1673-5374.357915

Date of submission: May 1, 2022

Date of decision: July 26, 2022

Date of acceptance: August 27, 2022

Date of web publication: October 11, 2022

From the Contents

Graphical Abstract

Ginsenoside Rb1 (G-Rb1) promotes metabolic reprogramming and inhibits oxidative stress through sirtuin 3 (Sirt3) to treat spinal cord injury

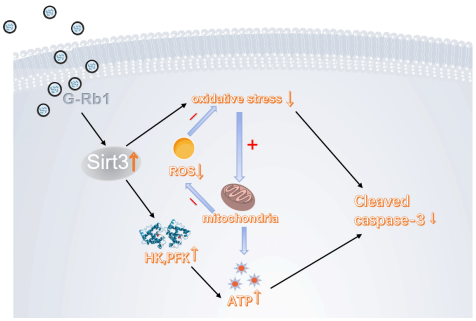

Abstract

Mitochondrial damage caused by oxidative stress and energy deficiency induced by focal ischemia and hypoxia are important factors that aggravate diseases. Studies have shown that ginsenoside Rb1 has neurotrophic and neuroprotective effects. However, whether it influences energy metabolism after spinal cord injury remains unclear. In this study, we treated mouse and cell models of spinal cord injury with ginsenoside Rb1. We found that ginsenoside Rb1 remarkably inhibited neuronal oxidative stress, protected mitochondria, promoted neuronal metabolic reprogramming, increased glycolytic activity and ATP production, and promoted the survival of motor neurons in the anterior horn and the recovery of motor function in the hind limb. Because sirtuin 3 regulates glycolysis and oxidative stress, mouse and cell models of spinal cord injury were treated with the sirtuin 3 inhibitor 3-TYP. When Sirt3 expression was suppressed, we found that the therapeutic effects of ginsenoside Rb1 on spinal cord injury were remarkably inhibited. Therefore, ginsenoside Rb1 is considered a potential drug for the treatment of spinal cord injury, and its therapeutic effects are closely related to sirtuin 3.

Key Words: axon growth; ginsenoside Rb1; glycolysis; metabolic reprogramming; mitochondrion; neuroprotection; oxidative stress; oxygen and glucose deprivation; Sirt3; spinal cord injury

Introduction

Spinal cord injury (SCI) is a central nervous system disease with a high incidence and disability rate (Wen et al., 2021). It not only causes patients to lose their working ability but also poses a significant burden to their families and society (Hu et al., 2021). SCI is mainly divided into primary and secondary injuries. Vascular damage and progressive edema caused by the primary injury continuously aggravate ischemia and hypoxia at the injury site, resulting in insufficient neuronal energy production and apoptosis (Jeong et al., 2021; Masterman and Ahmed, 2021; Shao et al., 2021; Wahyudi et al., 2022). Secondary injury is the continuation of the primary injury. Its pathological process mainly includes oxygen-free radical formation, local ischemia, and inflammatory reactions, which can last for weeks or months, resulting in the gradual expansion of the lesion area and further aggravation of nerve injury (Orr and Gensel, 2018; Jia et al., 2019; Zhou et al., 2020; Huang et al., 2021b). In particular, ischemia, hypoxia, and oxidative stress are considered key to the prognosis of SCI.

Panax ginseng is a commonly used Chinese medicinal herb, the root or stem of which has been used for the treatment of cardiovascular disease in several Asian countries (Lou et al., 2021). Pharmacological studies have shown that Panax ginseng and its extracts exert multiple pharmacological activities, such as antioxidative, platelet aggregation-inhibiting, and neuronal apoptosis-suppressing effects (Kiefer and Pantuso, 2003; Mancuso and Santangelo, 2017; Xie et al., 2018; Lou et al., 2021). Ginsenoside Rb1 (G-Rb1) is a tetracyclic triterpenoid mainly obtained from the roots or stems of Panax notoginseng and ginseng by extraction and purification (Lou et al., 2021). It is one of the main bioactive compounds of ginseng with minimal toxicity and neurotrophic and neuroprotective effects on brain injury (Chen et al., 2019; Zhang et al., 2021a, b). G-Rb1 promotes hippocampal nerve regeneration, enhances learning and memory, and has anti-aging and anti-fatigue effects (Cheng et al., 2005; Li et al., 2015; Zhao et al., 2018; Lin et al., 2019; Yang et al., 2020). In addition, it activates antioxidants, stimulates the immune system, has anti-apoptotic activity, and maintains cell adenosine triphosphate (ATP) levels (Fan et al., 2020). Moreover, some studies have reported that GRb1 potentially inhibits oxidative stress-induced apoptosis after SCI (Liu et al., 2018; Ye et al., 2019). However, there are limited studies related to the effects of GRb1 on energy metabolism in SCI.

As one of the most important deacetylases, sirtuin 3 (Sirt3) is essential for eukaryotic life and is closely related to metabolism in several organs (Zhang et al., 2020). Moreover, Sirt3 is involved in almost all aspects of mitochondrial metabolism and homeostasis *in vivo*, protecting mitochondria from various types of damage (Hirschey, 2011; Wang et al., 2019). However, its role in SCI has been less reported.

In this study, we aimed to identify an approach for treating SCI that may provide ideas for clinical treatment. To this end, we established a mouse model of blunt SCI and evaluated the therapeutic effect of G-Rb1 using behavioral assays. Then, the role of G-Rb1 in oxidative stress was assessed with mitochondrial probes and oxidative stress-related kits. The role of G-Rb1 in energy metabolism was evaluated by measuring the mitochondrial membrane potential, activity of key enzymes involved in glucose metabolism, and ATP content. Finally, a Sirt3 inhibitor was used to explore the molecular mechanism of G-Rb1 action.

[1]Department of Orthopedics, Third Affiliated Hospital of Jinzhou Medical University, Jinzhou, Liaoning Province, China; [2]Key Laboratory of Medical Tissue Engineering of Liaoning Province, Jinzhou Medical University, Jinzhou, Liaoning Province, China; [3]Pharmacy School, Jinzhou Medical University, Jinzhou, Liaoning Province, China
*Correspondence to: Xi-Fan Mei, PhD, meixifan@jzmu.edu.cn.
https://orcid.org/0000-0002-4452-8005 (Xi-Fan Mei)

Funding: *This work was supported by the National Natural Science Foundation of China, Nos. 81871556, 82072165; and Liaoning Revitalization Talents Program, No. XLYC1902108 (all to XFM).*

How to cite this article: *Wen S, Zou ZR, Cheng S, Guo H, Hu HS, Zeng FZ, Mei XF (2023) Ginsenoside Rb1 improves energy metabolism after spinal cord injury. Neural Regen Res 18(6):1332-1338.*

Methods

Animals and surgical procedures

C57BL/6J mice (male and female, 25–30 g, 6–8 weeks old) used in this study were purchased from Liaoning Changsheng Biotechnology Co., Ltd. (Benxi, China; license No. SCXK (Liao) 2020-0001). These mice were reared in the Experimental Animal Center of Jinzhou Medical University in a specific-pathogen-free environment at 22 ± 2°C and a 12-hour light-dark cycle (six mice per cage). All operations were approved by the Animal Care Committee of Jinzhou University (approval No. SYXK 2019-0007) in January 2021. All experiments were designed and reported according to the Animal Research: Reporting of *In Vivo* Experiments (ARRIVE) guidelines (Percie du Sert et al., 2020). Mice were divided into the Sham (n = 30), SCI (n = 57), G-Rb1 (SCI + 30 mg/kg G-Rb1, n = 57), and Sirt3^{-} (SCI + Sirt3 inhibitor + 30 mg/kg G-Rb1, n = 30) groups.

According to previous reports (Liu et al., 2020; Huang et al., 2021a; Lin et al., 2021), after mice were anesthetized with uratan (30 mg/kg, intraperitoneal injection, Sinopharm Chemical Reagent Co., Ltd. Shanghai, China), the back hair was removed, and the back was disinfected with povidone-iodine (LIRCON, Dezhou, Shandong, China). T9/T10 laminectomy was performed to expose the thoracic spinal cord. Next, a self-made impactor (12.5 g) was used to impact the exposed dorsal surface of the spinal cord from a height of 2 cm (Hu et al., 2021). The sham group was only stripped of the lamina but did not receive spinal cord blows. One hour after surgery, mice were injected intraperitoneally with G-Rb1 (30 mg/kg) dissolved in normal saline or saline (0.1 mL) for 7 days (Ye et al., 2019; Jiang et al., 2021; Zhang et al., 2021a). The Sirt3 inhibitor 3-(1H-1,2,3-triazol-4-yl) pyridine (3-TYP) was intraperitoneally injected at a dose of 50 mg/kg every 2 days for three doses 1 week before the surgery. On postoperative day 7, tissues were obtained (**Figure 1**).

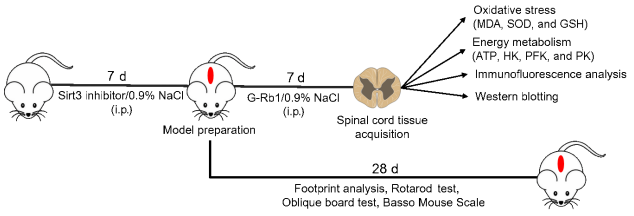

Figure 1 | **Animal experiment flow chart.**
ATP: Adenosine triphosphate; G-Rb1: ginsenoside Rb1; GSH: glutathione; HK: hexokinase; i.p.: intraperitoneal injection; MDA: malondialdehyde; PFK: phosphofructokinase; PK: pyruvate kinase; Sirt3: Sirtuin 3; SOD: superoxide dismutase.

Cell culture and model construction

PC12 cells (Cat# ab279978, RRID: CVCL_0481), as a commonly used neuronal cell line, were obtained from Abcam. Before the experiment, immunofluorescence was performed to confirm that cells were NeuN positive and that their morphology was consistent with PC12 cell characteristics. All cells were cultured at 37°C in a humidified atmosphere of 5% CO_2 and digested with 0.25% trypsin (Bioind, Shanghai, China) during cell subculture. The medium was Dulbecco's modified Eagle medium (Gibco, Grand Island, NY, USA) containing fetal bovine serum (10%), penicillin (100 U/mL), and streptomycin (100 μg/mL; Gibco).

For oxygen and glucose deprivation (OGD) (Wang et al., 2022), PC12 cells of a suitable density were selected, and their medium was changed to phosphate-buffered saline (PBS, pH 7.4). The hypoxia incubator was then filled with nitrogen gas (20 L/minute, 5 minutes) to maintain the oxygen concentration below 1%. After 2 hours of hypoxia and glucose deprivation, cells were removed from the hypoxic incubator and cultured in normal growth medium for 1 day (Jia et al., 2022). The control group was incubated normally. Cells were incubated with 100 μM G-Rb1 (Aladdin Chemical Reagent Co., Shanghai, China) for 1 day after OGD treatment. Cells were treated with the SIRT3 inhibitor 3-TYP (50 μM; MedChemExpress, Monmouth Junction, NJ, USA, Cat# HY-108331) for 3 hours before OGD. The concentrations of G-Rb1 *in vitro* were determined by 3-(4,5-dimethylthiazol-2-yl)-2,5-diphenyltetrazolium bromide (MTT) assays (**Additional Figure 1**).

Western blotting

After mice were subjected to different treatments for 7 days, they were anesthetized by an overdose of uratan. The spinal cord tissue (1 cm around the injury site) was collected, and proteins were extracted using radioimmunoprecipitation assay lysis buffer. Proteins were separated by sodium dodecyl sulfate-polyacrylamide gel electrophoresis after adding equal amounts of samples from different groups to a sodium dodecyl sulfate-polyacrylamide gel. Then, the proteins were transferred to polyvinylidene fluoride membranes. Subsequently, polyvinylidene fluoride membranes were blocked with 5% nonfat dry milk for 2 hours and incubated with primary antibodies overnight at 4°C. To detect apoptosis and axon regeneration, the primary antibodies and dilutions were as follows: anti-Bcl-2 (rabbit, 1:1000, Abcam, Cambridge, UK, Cat# 1017-1, RRID: AB_289591), anti-Bax (rabbit, 1:1000, Abcam, Cat# 1063-1, RRID: AB_351500), anti-cleaved caspase-3 (rabbit, 1:1000, Abcam, Cat# ab52293, RRID: AB_873720), anti-β-actin (mouse, 1:2000, Proteintech, Rosemont, IL, USA, Cat# 66009-1-Ig, RRID: AB_2687938), anti-growth associated protein-43 (GAP43; rabbit, 1:1000, Abcam, Cat# 3857-1, RRID: AB_10900622), and anti-neurofilament 70/200 kDa (NF200; mouse, 1:1000, Thermo Fisher Scientific, Waltham, MA, USA, Cat# MA5-15234, RRID: AB_10982518). The next day, the secondary antibody (horseradish peroxidase [HRP]-conjugated AffiniPure Goat Anti-Mouse IgG, Proteintech, Cat# SA00012-7, RRID:AB_2890970; HRP-conjugated AffiniPure Goat Anti-Rabbit IgG, Proteintech, Cat# SA00001-2, RRID:AB_2722564, both 1:1000) was incubated at 37°C for 2 hours. Finally, the optical densities were measured using a Tanon 5500 gel imaging system (Tanon, Shanghai, China). ImageJ V1.8.0 software (National Institutes of Health, Bethesda, MD, USA) (Schneider et al., 2012) was used to analyze signal intensities.

Immunofluorescence analysis

Mice were anesthetized by uratan and fully perfused with saline and 4% paraformaldehyde. Spinal cord tissue (1 cm around the injury site) was collected and placed in sucralose, and frozen sections were made. Frozen sections of spinal cords from different groups were washed with PBS until use. After permeabilizing with 0.3% Triton X-100 for 15 minutes, sections were blocked with goat serum (ZSGB-BIO, Beijing, China) for 2 hours. Subsequently, primary antibodies (anti-NeuN, mouse, 1:1000, Abcam, Cambridge, UK, Cat# ab77315, RRID: AB_1566475 and anti-cleaved caspase-3, 1:300) were incubated with sections overnight at 4°C. The next day, the corresponding secondary antibody (Alexa Fluor 488 goat anti-mouse IgG, Thermo Fisher Scientific, Waltham, MA, USA, Cat# A32728, RRID: AB_2633277; Alexa Fluor 568 goat anti-rabbit IgG, Thermo Fisher Scientific, Cat# A-11011, RRID: AB_143157, both 1:1000) was added and incubated at 37°C for 2 hours. Finally, sections were stained for 15 minutes using 4′,6-diamidino-2-phenylindole (DAPI) staining solution (Beyotime Biotechnology Co., Shanghai, China, Cat# C1002) containing an anti-quencher reagent and photographed with an FV10I confocal microscope. The fluorescence intensity in each group was analyzed with ImageJ software.

Cell samples were processed similarly to tissues. Briefly, cells subjected to different treatments were fixed with 4% polyfluoroalkyl for 30 minutes and then incubated with permeabilizing solution (0.1% Triton X-10) for 15 minutes, blocking solution (goat serum) for 2 hours, primary antibody (anti-β-tubulin: mouse, 1:300, Proteintech, Cat# 10094-1-AP, RRID: AB_2210695; anti-cleaved caspase-3: 1:100; anti-Sirt3: rabbit, 1:500, Abcam, Cat# 27-579, RRID: AB_10943254) for 18 hours at 4°C, secondary antibody (Alexa Fluor 488 goat anti-mouse IgG and Alexa Fluor 568 goat anti-rabbit IgG, both 1:1000) for 2 hours at 25°C, and nuclear staining solution (DAPI) for 30 minutes at 25°C. Finally, the fluorescence intensity was observed with a confocal laser scanning microscope (CLSM, BioTek Instruments, Winooski, VT, USA).

Determination of energy metabolism

After C57BL/6J mice were treated for 7 days, the spinal cord tissue (1 cm around the injury site) was collected. Cells were isolated 1 day after the completion of the corresponding treatment.

ATP content

ATP in spinal cord tissues/PC12 cells of different groups was extracted using an ATP detection kit, and then 100 μL of ATP detection working solution (Beyotime Biotechnology Co., Cat# S0027) was added to each well. After 5 minutes of incubation at room temperature, 20 μL of the sample or standard were added. Then, relative light unit values were determined using a microplate reader (Versa Max, Molecular Devices, Sunnyvale, CA, USA). Finally, the relative light unit values of ATP standards with different concentrations were detected, the standard curve was generated, and the ATP content in the sample was calculated.

Hexokinase activity

Hexokinase (HK) was extracted from spinal cord tissue/PC12 cells using a hexokinase assay kit (Beyotime, BC0745). After homogenizing samples in an ice bath, they were centrifuged at 8000 × g for 10 minutes at 4°C, and the supernatant was collected. Next, 180 μL of the reaction system, 10 μL of the reaction substrate, and 10 μL of the sample were added to a 96-well plate and mixed. The absorbance value A1 at 340 nm was immediately recorded for 20 seconds. After 5 minutes, the absorbance value A2 at 340 nm was recorded. Finally, HK activity was calculated following the kit's instructions.

Phosphofructokinase activity

Phosphofructokinase (PFK) was extracted from spinal cord tissue/PC12 cells using a PFK assay kit (Beyotime, BC0535). After homogenizing samples in an ice bath, they were centrifuged at 8000 × g for 10 minutes at 4°C, and the supernatant was collected. Next, 170 μL of the reaction system, 10 μL of the reaction substrate, 10 μL of iron supplement, and 10 μL of the sample were added to a 96-well plate and mixed. The absorbance value A1 at 340 nm was immediately recorded for 20 seconds. After 10 minutes, the absorbance value A2 at 340 nm was recorded. Finally, PFK activity was calculated following the kit's instructions.

Pyruvate kinase activity

Pyruvate kinase (PK) was extracted from spinal cord tissue/PC12 cells using a PK assay kit (Beyotime, BC0745). After homogenizing samples in an ice bath, they were centrifuged at 8000 × g for 10 minutes at 4°C, and the supernatant

was collected. Then, 180 μL of the reaction system, 10 μL of the reaction substrate, and 10 μL of the sample were added to a 96-well plate and mixed. The absorbance value A1 at 340 nm was immediately recorded for 20 seconds. After 2 minutes, the absorbance value A2 at 340 nm was recorded. Finally, PK activity was calculated following the kit's instructions.

Oxidative stress experiments
PC12 cells were seeded in 24-well plates and allowed to adhere. When the groups finished processing for 1 day, the reactive oxygen species (ROS) fluorescent probe 2,7-dichlorodihydrofluorescein diacetate (Beijing Solarbio Science & Technology Co., Beijing, China, Cat# CA1410) was added to different groups of cells and incubated in the incubator for 30 minutes. Finally, cells were observed and photographed using a fluorescence microscope (Leica, Wetzlar, Germany).

Superoxide dismutase (SOD; Beijing Solarbio Science & Technology Co., Cat# BC0175), plasma glutathione peroxidase (GSH-Px), and malondialdehyde (MDA; Beijing Solarbio Science & Technology Co., Cat# BC0025) detection kits were used to detect SOD activity, GSH-Px levels, and MDA contents in accordance with the manufacturer's instructions.

Measurement of mitochondrial membrane potential
PC12 cells were seeded in confocal plates and allowed to adhere. Then, the mitochondrial membrane potential probe JC-1 (Beyotime Biotechnology Co., Cat# C2003S) was added to different groups of cells following the manufacturer's instructions (Solarbio, Beijing, China). Finally, cells were observed and photographed using a fluorescence microscope.

Behavioral assessments
Footprint analysis
To detect the hind limb mobility of mice, a footprint analysis was performed. After 28 days of different treatments, the forelimbs were painted with black dye, and the hind limbs were painted with red dye. Mice were placed on absorbent paper surrounded by wooden boards and encouraged to walk in a straight line. The step length and step width were measured (Hu et al., 2021).

Rotarod test
The rotarod test was selected to assess the overall motor ability of mice. After 28 days of treatment, the mice were trained to stay on the rolling device (Ugo Basile, 47650, Gemonio, Italy) and slowly rotate a rod with a diameter of 2 cm at a speed of 5 revolutions/minute and an acceleration of 1 revolution/minute. The time spent on the stick until each mouse fell was recorded (Gong et al., 2022).

Oblique board test
At 1, 3, 5, 7, 14, 21, and 28 days after the operation, mice were placed on an inclined board (self-made), and the inclination angle was continuously increased at a speed of 0.5 °/s until the mice fell off. When the mouse slid down, the tilt angle of the slanted plate was recorded (Shen et al., 2019).

Basso Mouse Scale
Behavior was assessed using the Basso Mouse Scale (BMS). Mice were evaluated in a double-blind manner by three examiners at 1, 3, 5, 7, 10, 14, and 28 days after surgery. The BMS score ranges between 0 and 9, with 0 indicating no ankle activity and 9 indicating completely normal activity (Ge et al., 2021).

Statistical analysis
All animal and cell experiments were biologically repeated three times. The evaluators were blinded to the assignments. Statistical analysis was performed using GraphPad Prism (version 8.0.2, GraphPad Software, San Diego, CA, USA, www.graphpad.com), and all data were reported as the mean ± standard deviation. For analyzing the differences in BMS scores between the groups over time, a two-way repeated measures analysis of variance with Bonferroni's *post hoc* correction was performed. Other data were analyzed using a one-way analysis of variance with Tukey's multiple comparison test. All tests were two sided, and the level of significance was set at 0.05.

Results

G-Rb1 improves the motor function of mice
To detect the effect of G-Rb1 on the motor function of mice with SCI, we used footprint analysis, rotarod system tests, oblique board tests, and BMS scores to evaluate the motor function of mouse hind limbs. The footprint analysis showed that compared with footprints in the SCI group, footprints in the G-Rb1 group were improved, the step length was longer, and the step width was shorter (**Figure 2A–C**). The rotarod test found that the exercise time of the G-Rb1 group on the rolling axis was longer than that of the SCI group (**Figure 2D**). The oblique board test showed that the inclination angle of the inclined plate in the G-Rb1 group was greater than that in the SCI group (**Figure 2E**). Finally, the activity of the hind limbs of mice in each group was evaluated using the BMS score. The results showed that the movement of hind limbs in the G-Rb1 group was improved (**Figure 2F**). The above experiments comprehensively demonstrated the improvement in motor function of mice. Furthermore, immunofluorescence results showed that after treatment, anterior horn motoneuronal survival was higher in the G-Rb1 group than in the SCI group, and motoneurons were more morphologically intact (**Figure 2G** and **H**).

G-Rb1 inhibits oxidative stress and protects mitochondria after SCI
After SCI, mitochondria are severely injured, and their energy production is decreased, with increased production of ROS (Slater et al., 2022). G-Rb1 has antioxidant activity in myocardial ischemia (Fan et al., 2020), but whether it protects mitochondria through its antioxidant effects after SCI is unclear. First, a mitochondrial probe was used to detect the number of mitochondria in PC12 cells. The results showed that the number of mitochondria in neurons was increased after treatment (**Figure 3A** and **B**). To measure the oxidative stress in each group, ROS, MDA, SOD, and GSH-Px kits were used to detect the content of key substances involved in oxidative stress. The results showed that the level of ROS in neurons in the G-Rb1 group was lower than that in the OGD group (**Figure 3C** and **D**). MDA reflects the status of lipid peroxidation (Qi et al., 2014), and its content in neurons was also decreased after treatment (**Figure 3E**). The content of antioxidant SOD and activity of GSH-Px were increased after treatment (**Figure 3F** and **G**). To further verify the antioxidative stress activity of G-Rb1 *in vivo*, ROS, MDA, SOD, and GSH-Px kits were used to detect oxidative stress at the injury site (**Figure 3H–J**). Consistent with the *in vitro* findings, the G-Rb1 group showed decreased contents of ROS and MDA compared with the SCI group. Moreover, the G-Rb1 group exhibited increased SOD contents and GSH-Px activity compared with the SCI group. Therefore, G-Rb1 protected the mitochondria of neurons by inhibiting oxidative stress.

G-Rb1 improves energy deficiency and neuronal apoptosis after SCI
G-Rb1 has been reported to have therapeutic effects on ischemic diseases, such as myocardial ischemia and cerebral ischemia (Slater et al., 2022). Therefore, we considered whether its efficacy is related to the improvement in cell metabolism. First, we collected samples from damaged spinal cord tissue. After G-Rb1 treatment, ATP production in the injured spinal cord was increased (**Figure 4A**). ATP and lactic acid produced by glycolysis play an important role in neuronal apoptosis and axonal regeneration (Schurr and Passarella, 2022). Therefore, we next detected the activities of key glycolytic enzymes. The results showed that the activities of HK and PFK but not PK were increased by G-Rb1 (**Figure 4B–D**). Because neurons mediate spinal cord signaling (Ding et al., 2022), PC12 cells were used in all cell experiments. The results were similar to those in animal experiments (**Figure 4E–H**). Furthermore, using an optical microscope, we found that the axon length of neurons was increased after treatment. Moreover, the cell morphology was improved, and the cell density was increased (**Figure 4I**). To examine axon regeneration, the protein levels of GAP43 and NF200 were detected, and the western blot results showed that the levels of GAP3 and NF200 in the G-Rb1 group were higher than those in the SCI group (**Figure 4K–M**). Owing to the improvement in cell morphology and cell density after treatment, we speculate that G-Rb1 is related to the inhibition of apoptosis. Therefore, immunofluorescence staining was performed to detect apoptosis-related proteins, and the results showed that the fluorescence intensity of cleaved caspase-3 in the G-Rb1 group was lower than that in the SCI group in spinal cord tissues. In conclusion, G-Rb1 may reduce neuronal apoptosis by improving energy deficiency (**Figure 4N**).

Sirt3 is a key factor in the G-Rb1-mediated treatment of SCI
Because Sirt3 regulates glycolysis and oxidative stress (He et al., 2017; Zheng et al., 2018), we questioned whether G-Rb1 works through Sirt3. First, immunofluorescence was used to detect the expression of Sirt3. The results showed that Sirt3 was expressed in neurons, and the fluorescence intensity in the G-Rb1 group was higher than that in the OGD group (**Figure 5A** and **B**). The results of *in vivo* experiments showed that the protein expression of Sirt3 in the G-Rb1 group was also higher than that in the SCI group (**Figure 5C** and **D**). Next, the Sirt3 inhibitor and G-Rb1 were used together. The rotarod test showed that when the Sirt3 inhibitor was used with G-Rb1, the duration of the $Sirt3^{-}$ group on the rotarod was shorter than that of the G-Rb1 group (**Figure 5E**). Footprint analysis also showed that the step length of the Sirt3- group was shorter, and the step width was longer compared with those in the G-Rb1 group (**Figure 5F–H**). Additionally, the results of the oblique board test showed that the grasping ability of the Sirt3- group was weaker than that of the G-Rb1 group (**Figure 5I**). The BMS score revealed that the hind limb motor ability of the Sirt3- group was lower than that of the G-Rb1 group (**Figure 5J**). Therefore, G-Rb1 promotes the recovery of motor ability in mice, which is related to Sirt3.

Sirt3 is key for G-Rb1 to inhibit oxidative stress in the treatment of SCI
The above experiments demonstrated that G-Rb1 inhibits neuronal oxidative stress and protects neuronal mitochondria. We next questioned whether it works through Sirt3. First, the functional status of mitochondria was detected by JC-1. Compared with the G-Rb1 group, the $Sirt3^{-}$ group showed decreased red/green fluorescence intensity in PC12 cells, suggesting the aggravation of mitochondrial damage (**Figure 6A** and **B**). Moreover, the key substances of oxidative stress, such as MDA, SOD, and GSH-Px, in neurons of each group were detected. The results showed that after Sirt3 was inhibited, the MDA content was higher than that in the G-Rb1 group (**Figure 6C**). In addition, the SOD content and GSH-Px activity were decreased (**Figure 6D** and **E**). To confirm these results *in vivo*, we collected the injured tissues of mice in each group. The results also showed that when Sirt3 was inhibited, the MDA content was increased, and the SOD content and GSH-Px activity were decreased (**Figure 6F–H**). Therefore, Sirt3 is key for G-Rb1 to inhibit oxidative stress and protect mitochondria.

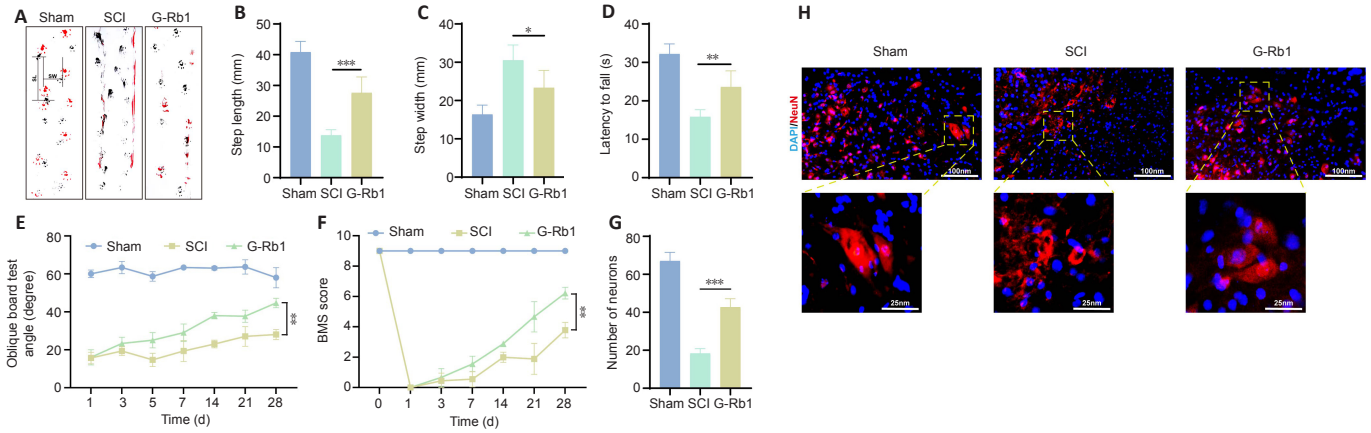

Figure 2 | **G-Rb1 improves the motor function of mice.**
(A–C) Footprint images of mice and statistical analysis of step width and step length 28 days after surgery. The footprint, step length, and step width of the G-Rb1 group were more similar to those of the Sham group. (D) Statistical analysis of mice falling from the rotarod 28 days after surgery. (E) Statistical analysis of the inclination angle of mice when they fell from the inclined plate 28 days after the operation. (F) BMS score of mice 28 days after surgery. (G, H) Confocal images of neurons (NeuN-positive cells, red, Alexa Fluor 568) in mouse spinal cord tissue at 28 days after surgery and statistical analysis of the number of neurons. The number of neurons in the G-Rb1 group was higher than that in the SCI group. All data are expressed as the mean ± SD (n = 3). *P < 0.05, **P < 0.01, ***P < 0.001 (BMS: two-way repeated measures analysis of variance followed by Bonferroni's *post-hoc* correction; other data: one-way analysis of variance followed by Tukey's multiple comparison test). BMS: Basso Mouse Scale; DAPI: 4′,6-diamidino-2-phenylindole; G-Rb1: Ginsenoside Rb1; SCI: spinal cord injury.

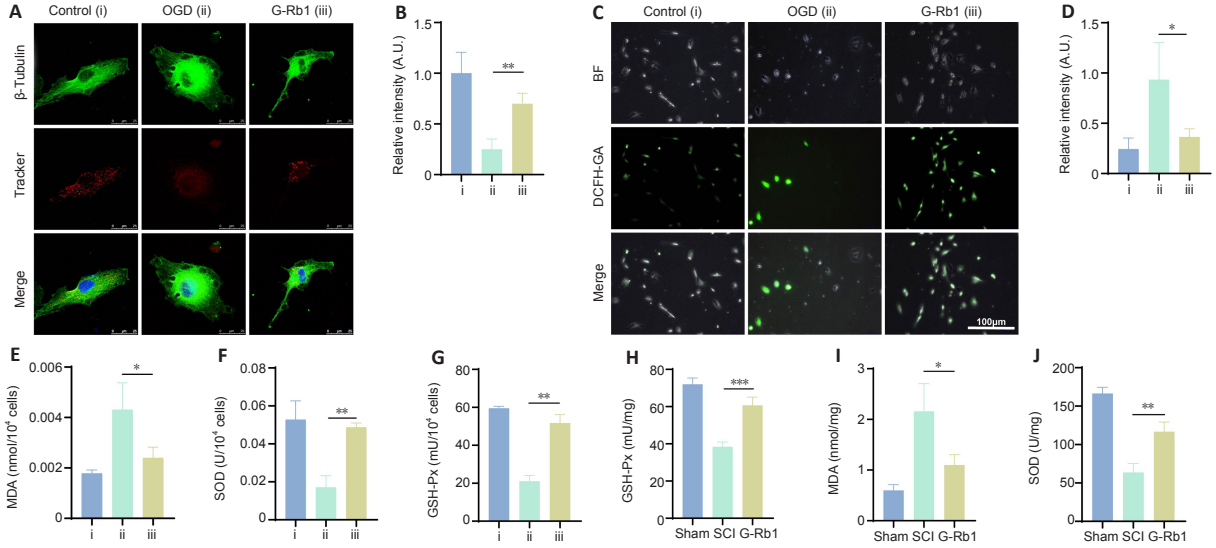

Figure 3 | **G-Rb1 inhibits oxidative stress and protects mitochondria after SCI.**
(A, B) Fluorescence images of mitochondria in different groups of PC12 cells are marked by the tracker. The red fluorescent signal represents mitochondria. Compared with the OGD group, the G-Rb1 group had more mitochondria. (C, D) Fluorescence images of different groups of PC12 cells labeled with the ROS probe (DCFH-DA). The green fluorescent signal represents ROS. Compared with that in the OGD group, the ROS content of the G-Rb1 group was lower. (E–G) The contents of MDA and SOD and the activity of GSH-Px in PC12 cells in different groups. (H–J) The content of MDA and SOD and the activity of GSH-Px in spinal cord tissues of different groups. All data are expressed as the mean ± SD. The experiment was repeated three times. *P < 0.05, **P < 0.01, ***P < 0.001 (one-way analysis of variance followed by Tukey's multiple comparison test). i, ii, and iii represent Control, OGD, and G-Rb1 groups, respectively. A.U.: Arbitrary unit; BF: brightfield; DCFH-DA: 2,7-dichlorodihydrofluorescein diacetate; G-Rb1: ginsenoside Rb1; GSH: glutathione; MDA: malondialdehyde; OGD: oxygen/glucose deprivation; SCI: spinal cord injury; SOD: superoxide dismutase.

Sirt3 is involved in the regulation of glycolysis by G-Rb1 in the treatment of SCI

Because Sirt3 is involved in the regulation of SCI recovery by G-Rb1, we next determined which regulatory processes Sirt3 plays a role in. First, Sirt3-inhibited SCI mice were treated with G-Rb1. ATP detection showed that the intracellular ATP content in the Sirt3- group was lower than that in the G-Rb1 group (**Figure 7A**). The results of enzyme activity experiments showed that compared with those in the G-Rb1 group, the activities of HK and PFK in the Sirt3- group were increased, but there was no difference in PK activity (**Figure 7B–D**). To clarify the effect of Sirt3 inhibition on neurons, PC12 cells were used to detect energy metabolism. The results showed that ATP production, HK activity, and PFK activity were decreased after Sirt3 inhibition (**Figure 7E–H**). To determine whether G-Rb1 inhibits neuronal apoptosis through metabolic reprogramming related to Sirt3, apoptosis-related proteins were detected. The immunofluorescence results showed that after Sirt3 inhibition, the fluorescence intensity of cleaved caspase-3 was higher than that in the G-Rb1 group (**Figure 7I–K**). In addition, the expression of Bax and cleaved caspase-3 was higher than that in the G-Rb1 group, and the expression of Bcl-2 was lower than that in the G-Rb1 group (**Figure 7L–O**). In conclusion, Sirt3 inhibition reverses the neuronal metabolic reprogramming and apoptosis caused by G-Rb1.

Discussion

SCI triggers oxidative stress, inhibits mitochondrial and glycolytic functions, induces apoptosis, and leads to secondary injury to the spinal cord (Ge et al., 2021). In this study, G-Rb1 improved the motor function of the hind limbs of SCI mice by inhibiting oxidative stress to protect mitochondria and increasing the activity of the key glycolysis enzymes HK and PFK to improve energy deficiency in the ischemic and hypoxic environment of lesions. Using a Sirt3 inhibitor, we determined that Sirt3 is a key factor in the efficacy of G-Rb1.

As the main active ingredient of ginseng, G-Rb1 has low toxicity and neurotrophic and neuroprotective effects on brain injury (Zhang et al., 2021a). This study found that G-Rb1 inhibited oxidative stress after SCI and promoted energy metabolism, thereby improving the motor function of the hind limbs of mice. Although G-Rb1 was less studied in SCI, it has been reported in various diseases, such as stroke, intestinal ischemia, and reperfusion. In a variety of stroke mice, G-Rb1 reduced neuronal death by scavenging free radicals (Xie et al., 2021). Furthermore, in an ischemic microenvironment, G-Rb1 reduces the concentration of glutamic acid and Ca^{2+} and inhibits the apoptosis of hippocampal pyramidal neurons (Wang et al., 2017; Guo et al., 2018). G-Rb1 also had a significant effect in other organ ischemia-reperfusion diseases. Sun et al. reported that after intestinal ischemia and reperfusion in rats, the

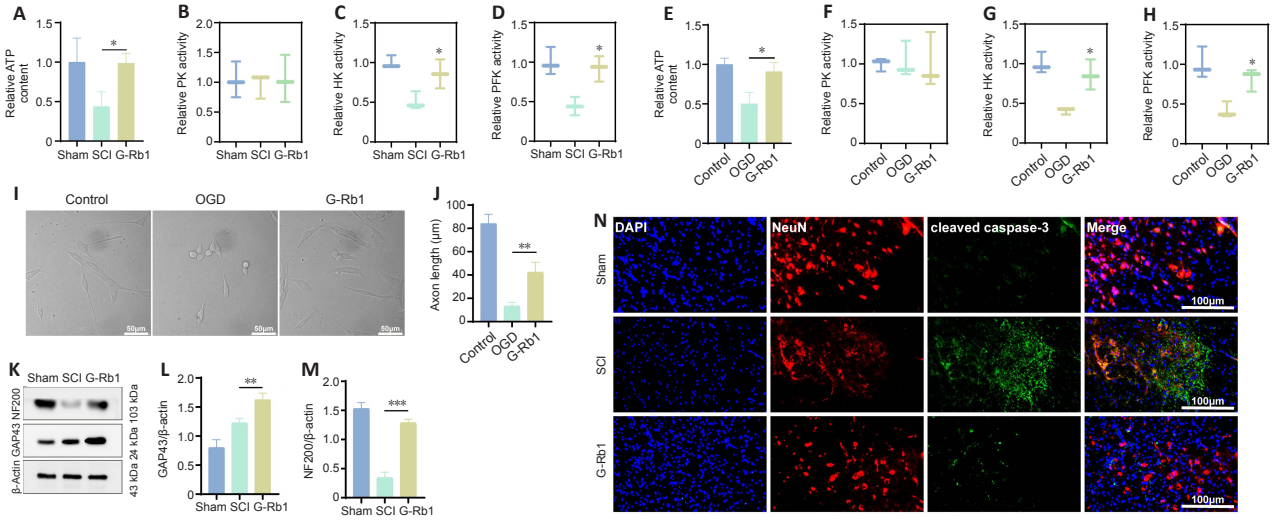

Figure 4 | G-Rb1 improves energy deficiency and neuronal apoptosis.
(A) Statistical analysis of the ATP content in spinal cord tissues of different groups. (B–D) Statistical analysis of PK, PFK, and HK activities in spinal cord tissues of different groups. (E) Statistical analysis of the ATP content in PC12 cells in different groups. (F–H) Statistical analysis of PK, PFK, and HK activities in different groups of PC12 cells. The data in A–D were normalized by the Sham group and the data in E–H were normalized by the control group. (I, J) Optical microscope image of different groups of PC12 cells and statistical analysis of axonal lengths. The axonal length in the G-Rb1 group was longer than that in the OGD group. (K–M) Western blot images and statistical analysis of the expression of NF200 and GAP43 in the spinal cord tissues of different groups. (O) Immunofluorescence images of cleaved caspase-3 (green, Alexa Fluor 568), an apoptosis protein, in spinal cord tissues. The fluorescence intensity of cleaved caspase-3 in the G-Rb1 group was lower than that in the SCI group. All data are expressed as the mean ± SD. The experiment was repeated three times. *P < 0.05, **P < 0.01, ***P < 0.001 (one-way analysis of variance followed by Tukey's multiple comparison test). ATP: Adenosine-triphosphate; DAPI: 4′,6-diamidino-2-phenylindole; G-Rb1: ginsenoside Rb1; GAP43: growth associated protein-43; HK: hexokinase; NF200: neurofilaments 200 kDa; OGD: oxygen and glucose deprivation; PFK: phosphofructokinase; PK: pyruvate kinase; SCI: spinal cord injury.

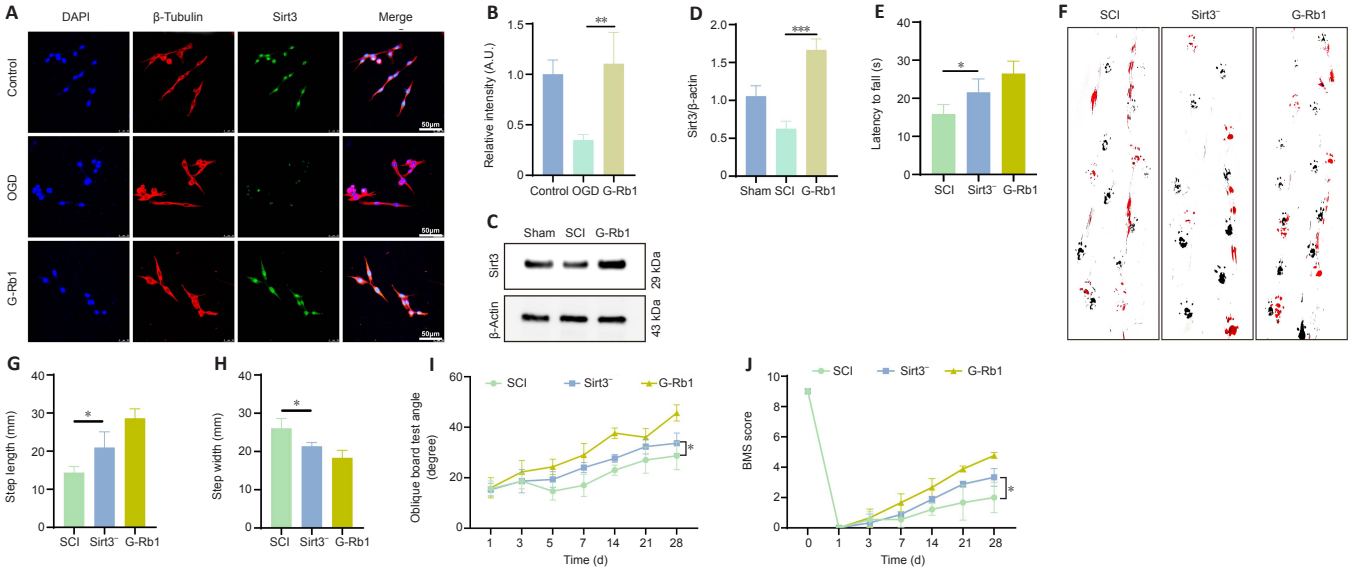

Figure 5 | Sirt3 is a key factor in the G-Rb1-mediated treatment of SCI.
(A, B) Immunofluorescence images and statistical analysis of Sirt3 expression in different groups of PC12 cells. Sirt3 (green, Alexa Fluor 488) is the target factor, and β-tubulin (red, Alexa Fluor 568) represents the cytoskeleton. The fluorescence intensity (normalized by the control group) of Sirt3 in the G-Rb1 group was higher than that in the OGD group. (C, D) Western blot images and statistical analysis of Sirt3 expression in spinal cord tissues of different groups. Sirt3 expression was normalized by β-actin. (E) Statistical analysis of mice falling from the rotarod 28 days after surgery. (F–H) Footprint images of mice and statistical analysis of step width and step length 28 days after surgery. (I) Statistical analysis of the inclination angle of mice when they fell from the inclined plate 28 days after the operation. (J) BMS score of mice 28 days after surgery. Data are expressed as the mean ± SD (n = 3). *P < 0.05, **P < 0.01, ***P < 0.001 (BMS: two-way repeated measures analysis of variance followed by Bonferroni's *post hoc* correction; other data: one-way analysis of variance followed by Tukey's multiple comparison test). i, ii, and iii represent SCI, Sirt3^{-}, and G-Rb1 groups, respectively. BMS: Basso Mouse Scale; G-Rb1: ginsenoside Rb1; OGD: oxygen and glucose deprivation; SCI: spinal cord injury; Sirt3: Sirtuin 3.

MDA content was increased, and SOD levels were decreased. G-Rb1 reduced oxidative substances and increased antioxidants, thereby reducing oxidative stress damage (Sun et al., 2013). In this study, G-Rb1 improved the hind limb function score in mice with SCI, reduced the MDA content, increased the SOD content and GSH-Px activity, protected damaged mitochondria, increased the activity of key glycolysis enzymes, and increased the ATP content at the site of injury. Its antioxidant stress mechanisms may include scavenging free radicals, increasing antioxidant enzyme activity, and blocking lipid peroxidation. Neuronal mechanisms to protect against ischemia and hypoxia at the site of injury include increased glycolysis and improvements in mitochondrial function after the inhibition of oxidative stress. Therefore, we speculate that the mechanism by which G-Rb1 improves the physiological function of spinal cord tissue is associated with the inhibition of oxidative stress and improvement in local energy supply deficiencies.

Sirt3 plays an important role in physiological processes, especially energy homeostasis and antioxidant stress (Wu et al., 2014). This study found that Sirt3 inhibition decreased the motor function of SCI mice treated with G-Rb1, increased the oxidative stress capacity, inhibited glycolysis, and decreased ATP production. Therefore, we speculate that Sirt3 is a key factor in the treatment of SCI with G-Rb1. First, Sirt3 has been demonstrated to inhibit oxidative stress in the central nervous system (Hou et al., 2022). As reported by Lee et al. (2021), the overexpression of Sirt3 mitigates oxidative stress-induced cell death and mitochondrial dysfunction in dopaminergic neurons and astrocytes. In Parkinson's disease, Sirt3-mediated inhibition of oxidative stress has been widely reported (Salvatori et al., 2017; Shen et al., 2020). Sirt3 modulates the activities and biological functions of a variety of proteins involved in various mitochondrial functions. Increasing numbers of studies have suggested that the upregulation of Sirt3 confers a beneficial effect on

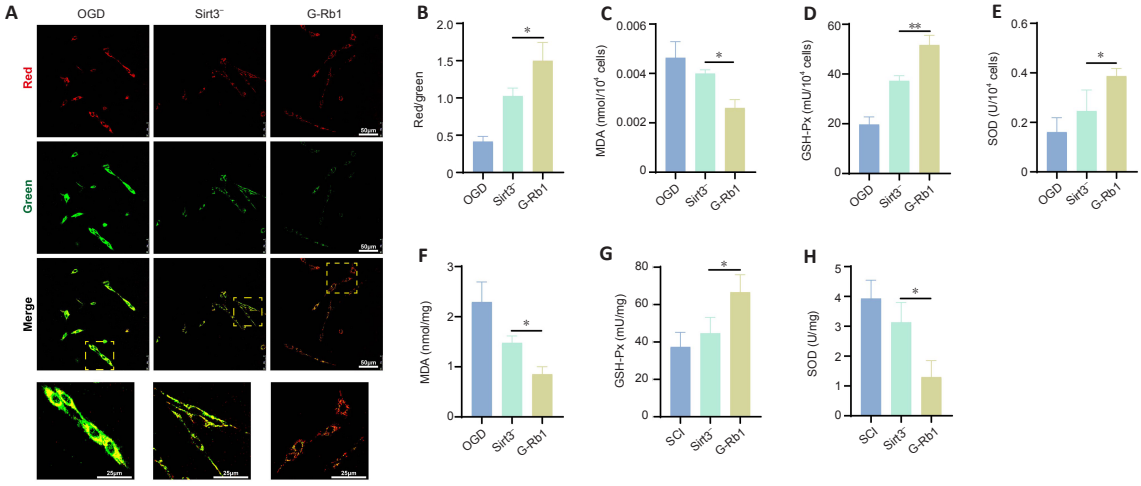

Figure 6 | **Sirt3 is key for G-Rb1 to inhibit oxidative stress in the treatment of SCI.**
(A, B) Fluorescence images in each group of PC12 cells labeled with the mitochondrial membrane potential probe JC-1 and the statistical analysis. The red/green value of the fluorescence signal in the G-Rb1 group was greater than that in the Sirt3- group. (C–E) The contents of MDA and SOD and the activity of GSH-Px in PC12 cells in each group. (F–H) The contents of MDA and SOD and the activity of GSH-Px in spinal cord tissues of different groups. All data are expressed as the mean ± SD. The experiment was repeated three times. *$P < 0.05$, **$P < 0.01$, ***$P < 0.001$ (one-way analysis of variance followed by Tukey's multiple comparison test). G-Rb1: Ginsenoside Rb1; GSH: glutathione; MDA: malondialdehyde; OGD: oxygen and glucose deprivation; SCI: spinal cord injury; Sirt3: Sirtuin 3; SOD: superoxide dismutase.

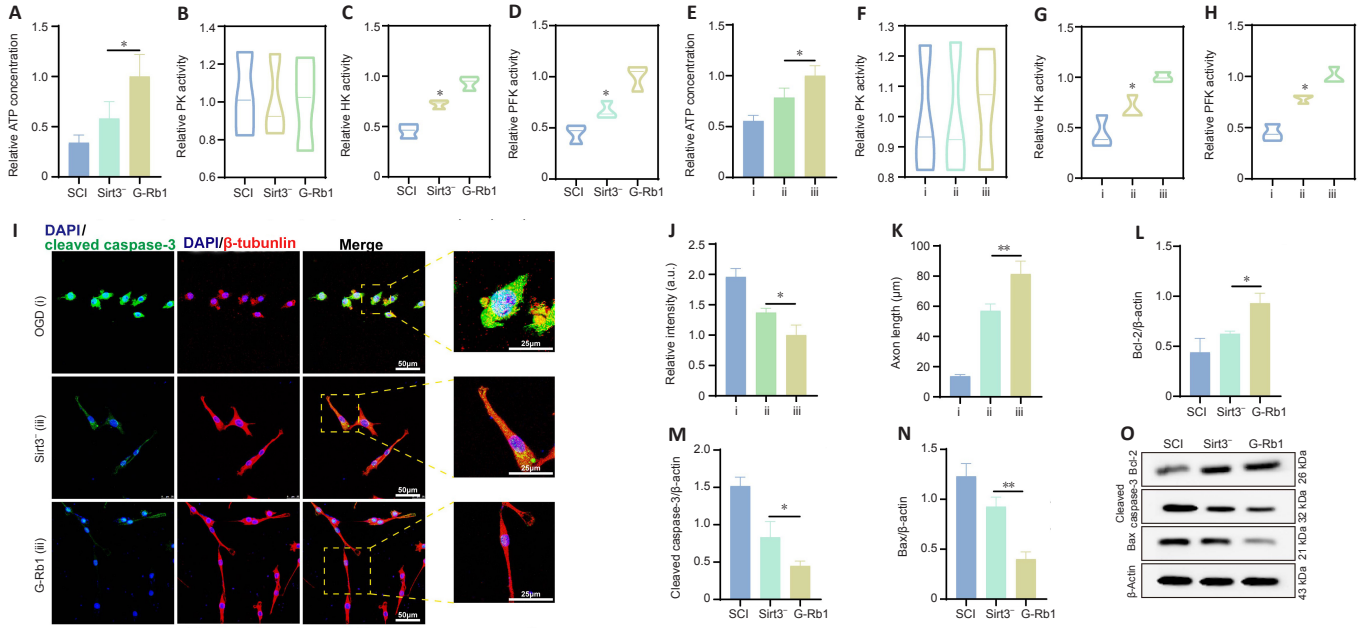

Figure 7 | **Sirt3 is involved in the regulation of glycolysis by G-Rb1 in the treatment of SCI.**
(A) Statistical analysis of the ATP content in spinal cord tissues of different groups. (B–D) Statistical analysis of PK, PFK, and HK activities in spinal cord tissues of different groups. (E) Statistical analysis of the ATP content in PC12 cells of different groups. (F–H) Statistical analysis of PK, PFK, and HK activities in different groups of PC12 cells. The data were normalized by the G-Rb1 group. (I–K) Immunofluorescence images of cleaved caspase-3 expression in different groups of PC12 cells and statistical analysis of the intensity and axon length. β-tubulin (red, Alexa Fluor 568) represents the cytoskeleton, and cleaved caspase-3 (green, Alexa Fluor 488) is a key apoptosis protein. The green fluorescence intensity of the G-Rb1 group was lower than that of the Sirt3⁻ group, and the length of axons was increased compared with that in the Sirt3⁻ group. (L–O) Western blot images and statistical analysis of Bcl-2, Bax, and cleaved caspase-3 expression in spinal cord tissues of different groups. The red fluorescent signal represents β-tubulin, and the green fluorescent signal represents cleaved caspase-3. The green fluorescence intensity of the G-Rb1 group was lower than that of the Sirt3⁻ group. All data are expressed as the mean ± SD. The experiment was repeated three times. *$P < 0.05$, **$P < 0.01$, ***$P < 0.001$ (one-way analysis of variance followed by Tukey's multiple comparison test). i, ii, and iii represent SCI, Sirt3⁻, and G-Rb1 groups, respectively. ATP: Adenosine-triphosphate; DAPI: 4′,6-diamidino-2-phenylindole; G-Rb1: Ginsenoside Rb1; HK: hexokinase; OGD: oxygen and glucose deprivation; PFK: phosphofructokinase; PK: pyruvate kinase; SCI: spinal cord injury; Sirt3: Sirtuin 3.

neuroprotection in various Parkinson's disease models (Salvatori et al., 2017). First, the antioxidant stress effects of Sirt3 protect mitochondria, thereby improving cellular energy metabolism (Zhai et al., 2017). In addition, Sirt3 regulates glycolysis (Li et al., 2020). After SCI, the injury is locally caused by severe ischemia and hypoxia, and mitochondrial damage and oxygen deficiency increase the importance of anaerobic respiration. This experiment found that Sirt3 increases the activities of key glycolysis enzymes and promotes the production of ATP. Recent studies have also reported a decrease in glycolytic activity and an increase in mitochondrial oxygen consumption in Sirt3-deficient endothelial cells (He et al., 2017; Zeng and Chen, 2019). In addition, Sirt3 deficiency inhibits the formation of HKII-VDAC-ANT complexes, resulting in decreased glycolytic enzyme activity, reduced glucose uptake, and increased conversion of metabolic substrates from glucose to fatty acids (Lantier et al., 2015). These reports suggest that Sirt3 not only has antioxidant stress effects but also improves resistance to ischemia and hypoxia damage through metabolic reprogramming that protects mitochondria and glycolysis.

In summary, G-Rb1 inhibits neural oxidative stress and increases energy production through Sirt3, thereby promoting recovery from SCI. These results provide guidance for the application of G-Rb1 in the clinical treatment of SCI. However, there are some shortcomings in this study. The energy metabolism system is large and complex. This study did not investigate the entire process of energy metabolism, and it is difficult to comprehensively explain the regulation of energy metabolism by G-Rb1. In future experiments, we will use a seahorse cell energy metabolism analyzer and metabolome sequencing technology to comprehensively detect the changes in energy metabolism.

Author contributions: *Study design and manuscript draft: SW; experiment implementation: SW, ZRZ, SC, HG; data analysis: ZRZ; technical assistance: HSH, FZZ; financial support and study guide: XFM. All authors have approved the final version of the manuscript.*

Conflicts of interest: *The authors declare that there are no competing financial interests.*

Availability of data and materials: *All data generated or analyzed during this study are included in this published article and its supplementary information files.*

Open access statement: *This is an open access journal, and articles are distributed under the terms of the Creative Commons AttributionNonCommercial-ShareAlike 4.0 License, which allows others to remix, tweak, and build upon the work non-commercially, as long as appropriate credit is given and the new creations are licensed under the identical terms.*

Additional file:

Additional Figure 1: *Determination of G-Rb1 concentration in vitro using MTT.*

References

Chen C, Zhang H, Xu H, Zheng Y, Wu T, Lian Y (2019) Ginsenoside Rb1 ameliorates cisplatin-induced learning and memory impairments. J Ginseng Res 43:499-507.
Cheng Y, Shen LH, Zhang JT (2005) Anti-amnestic and anti-aging effects of ginsenoside Rg1 and Rb1 and its mechanism of action. Acta Pharmacol Sin 26:143-149.
Ding LL, Hu SF, He XW, Zhang P, Zhao FF, Cheng LH, Huang BL, Liu TP, Zhang Q, He F, Hu SS, Zhang YJ, Yu Y, Xiong P, Wang CK (2022) Warm acupuncture therapy alleviates neuronal apoptosis after spinal cord injury via inhibition of the ERK signaling pathway. J Spinal Cord Med doi: 10.1080/10790268.2022.2088498.
Fan W, Huang Y, Zheng H, Li S, Li Z, Yuan L, Cheng X, He C, Sun J (2020) Ginsenosides for the treatment of metabolic syndrome and cardiovascular diseases: Pharmacology and mechanisms. Biomed Pharmacother 132:110915.
Ge MH, Tian H, Mao L, Li DY, Lin JQ, Hu HS, Huang SC, Zhang CJ, Mei XF (2021) Zinc attenuates ferroptosis and promotes functional recovery in contusion spinal cord injury by activating Nrf2/GPX4 defense pathway. CNS Neurosci Ther 27:1023-1040.
Gong J, Liu Y, Chung TH, Xu L, Lund TC, Chang LJ (2022) Intracerebral lentiviral ABCD1 gene therapy in an early disease onset ALD mouse model. Gene Ther doi: 10.1038/s41434-022-00355-0.
Guo Y, Wang LP, Li C, Xiong YX, Yan YT, Zhao LQ, Li SD, Sun J, Luo HY, Xian CJ (2018) Effects of ginsenoside Rb1 on expressions of phosphorylation akt/phosphorylation mTOR/phosphorylation PTEN in artificial abnormal hippocampal microenvironment in rats. Neurochem Res 43:1927-1937.
He X, Zeng H, Chen ST, Roman RJ, Aschner JL, Didion S, Chen JX (2017) Endothelial specific SIRT3 deletion impairs glycolysis and angiogenesis and causes diastolic dysfunction. J Mol Cell Cardiol 112:104-113.
Hirschey MD (2011) Old enzymes, new tricks: sirtuins are NAD(+)-dependent de-acylases. Cell Metab 14:718-719.
Hou M, Bao W, Gao Y, Chen J, Song G (2022) Honokiol improves cognitive impairment in APP/PS1 mice through activating mitophagy and mitochondrial unfolded protein response. Chem Biol Interact 351:109741.
Hu H, Xia N, Lin J, Li D, Zhang C, Ge M, Tian H, Mei X (2021) Zinc regulates glucose metabolism of the spinal cord and neurons and promotes functional recovery after spinal cord injury through the AMPK signaling pathway. Oxid Med Cell Longev 2021:4331625.
Huang HT, Tung TH, Lin M, Wang X, Li X, Liang K, Qian Q, Chen PE (2021a) Characterizing spatiotemporal progression and prediction of infarct lesion volumes in experimental acute ischemia using quantitative perfusion and diffusion imaging. Appl Radiat Isot 168:109522.
Huang N, Li S, Xie Y, Han Q, Xu XM, Sheng ZH (2021b) Reprogramming an energetic AKT-PAK5 axis boosts axon energy supply and facilitates neuron survival and regeneration after injury and ischemia. Curr Biol 31:3098-3114.e7.
Jeong HJ, Yun Y, Lee SJ, Ha Y, Gwak SJ (2021) Biomaterials and strategies for repairing spinal cord lesions. Neurochem Int 144:104973.
Jia G, Zhang Y, Li W, Dai H (2019) Neuroprotective role of icariin in experimental spinal cord injury via its antioxidant, anti-neuroinflammatory and anti-apoptotic properties. Mol Med Rep 20:3433-3439.
Jia X, Shao W, Tian S (2022) Berberine alleviates myocardial ischemia-reperfusion injury by inhibiting inflammatory response and oxidative stress: the key function of miR-26b-5p-mediated PTGS2/MAPK signal transduction. Pharm Biol 60:652-663.
Jiang L, Yin X, Chen YH, Chen Y, Jiang W, Zheng H, Huang FQ, Liu B, Zhou W, Qi LW, Li J (2021) Proteomic analysis reveals ginsenoside Rb1 attenuates myocardial ischemia/reperfusion injury through inhibiting ROS production from mitochondrial complex I. Theranostics 11:1703-1720.
Kiefer D, Pantuso T (2003) Panax ginseng. Am Fam Physician 68:1539-1542.
Lantier L, Williams AS, Williams IM, Yang KK, Bracy DP, Goelzer M, James FD, Gius D, Wasserman DH (2015) SIRT3 is crucial for maintaining skeletal muscle insulin action and protects against severe insulin resistance in high-fat-fed mice. Diabetes 64:3081-3092.
Lee S, Jeon YM, Jo M, Kim HJ (2021) Overexpression of SIRT3 suppresses oxidative stress-induced neurotoxicity and mitochondrial dysfunction in dopaminergic neuronal cells. Exp Neurobiol 30:341-355.
Li J, Liu H, Takagi S, Nitta K, Kitada M, Srivastava SP, Takagaki Y, Kanasaki K, Koya D (2020) Renal protective effects of empagliflozin via inhibition of EMT and aberrant glycolysis in proximal tubules. JCI Insight 5:e129034.
Li T, Shu YJ, Cheng JY, Liang RC, Dian SN, Lv XX, Yang MQ, Huang SL, Chen G, Yang F (2015) Pharmacokinetics and efficiency of brain targeting of ginsenosides Rg1 and Rb1 given as Nao-Qing microemulsion. Drug Dev Ind Pharm 41:224-231.
Lin J, Gao S, Wang T, Shen Y, Yang W, Li Y, Hu H (2019) Ginsenoside Rb1 improves learning and memory ability through its anti-inflammatory effect in Aβ(1-40) induced Alzheimer's disease of rats. Am J Transl Res 11:2955-2968.
Lin S, Zhou Z, Zhao H, Xu C, Guo Y, Gao S, Mei X, Tian H (2021) TNF promotes M1 polarization through mitochondrial metabolism in injured spinal cord. Free Radic Biol Med 172:622-632.
Liu R, Wu Z, Yu H (2020) Effect of different treatments on macrophage differentiation in chronic obstructive pulmonary disease and repeated pulmonary infection. Saudi J Biol Sci 27:2076-2081.
Liu X, Gu X, Yu M, Zi Y, Yu H, Wang Y, Xie Y, Xiang L (2018) Effects of ginsenoside Rb1 on oxidative stress injury in rat spinal cords by regulating the eNOS/Nrf2/HO-1 signaling pathway. Exp Ther Med 16:1079-1086.
Lou T, Huang Q, Su H, Zhao D, Li X (2021) Targeting Sirtuin 1 signaling pathway by ginsenosides. J Ethnopharmacol 268:113657.
Mancuso C, Santangelo R (2017) Panax ginseng and Panax quinquefolius: From pharmacology to toxicology. Food Chem Toxicol 107:362-372.
Masterman E, Ahmed Z (2021) Experimental treatments for oedema in spinal cord injury: a systematic review and meta-analysis. Cells 10:2682.
Orr MB, Gensel JC (2018) Spinal cord injury scarring and inflammation: therapies targeting glial and inflammatory responses. Neurotherapeutics 15:541-553.
Percie du Sert N, Hurst V, Ahluwalia A, Alam S, Avey MT, Baker M, Browne WJ, Clark A, Cuthill IC, Dirnagl U, Emerson M, Garner P, Holgate ST, Howells DW, Karp NA, Lazic SE, Lidster K, MacCallum CJ, Macleod M, Pearl EJ, et al. (2020) The ARRIVE guidelines 2.0: Updated guidelines for reporting animal research. PLoS Biol 18:e3000410.
Qi B, Zhang L, Zhang Z, Ouyang J, Huang H (2014) Effects of ginsenosides-Rb1 on exercise-induced oxidative stress in forced swimming mice. Pharmacogn Mag 10:458-463.
Salvatori I, Valle C, Ferri A, Carrì MT (2017) SIRT3 and mitochondrial metabolism in neurodegenerative diseases. Neurochem Int 109:184-192.
Schneider CA, Rasband WS, Eliceiri KW (2012) NIH Image to ImageJ: 25 years of image analysis. Nat Methods 9:671-675.
Schurr A, Passarella S (2022) Aerobic glycolysis: a deoxymoron of (neuro)biology. Metabolites 12:72.
Shao M, Zheng C, Ma X, Lyu F (2021) Ecto-5'-nucleotidase (CD73) inhibits dorsal root ganglion neuronal apoptosis by promoting the Ado/cAMP/PKA/CREB pathway. Exp Ther Med 22:1374.
Shen Q, Cao Y, Xia Y (2019) Atorvastatin attenuates spinal cord injury by chronic fluorosis in rats. Neuroreport 30:1256-1260.
Shen Y, Wu Q, Shi J, Zhou S (2020) Regulation of SIRT3 on mitochondrial functions and oxidative stress in Parkinson's disease. Biomed Pharmacother 132:110928.
Slater PG, Domínguez-Romero ME, Villarreal M, Eisner V, Larraín J (2022) Mitochondrial function in spinal cord injury and regeneration. Cell Mol Life Sci 79:239.
Sun Q, Meng QT, Jiang Y, Liu HM, Lei SQ, Su WT, Duan WN, Wu Y, Xia ZY, Xia ZY (2013) Protective effect of ginsenoside Rb1 against intestinal ischemia-reperfusion induced acute renal injury in mice. PLoS One 8:e80859.
Wahyudi, Islam AA, Hatta M, Adhimarta W, Faris M, Mustamir N, Bukhari A, Prihantono, Kaelan C, Hendarto J, Imran NH, Rosyidi RM (2022) The role of MLC901 in reducing VEGF as a vascular permeability marker in rats with spinal cord injury. Ann Med Surg (Lond) 75:103344.
Wang L, Song Z, Zou H, Chen H, Hu Y, Li X, Liu J (2022) CircRNA3616 knockdown attenuates inflammation and apoptosis in spinal cord injury by inhibiting TLR4/NF-κB activity via sponging miR-137. Mol Cell Biochem doi: 10.1007/s11010-022-04509-x.
Wang S, Li M, Guo Y, Li C, Wu L, Zhou XF, Luo Y, An D, Li S, Luo H, Pu L (2017) Effects of Panax notoginseng ginsenoside Rb1 on abnormal hippocampal microenvironment in rats. J Ethnopharmacol 202:138-146.
Wang T, Cao Y, Zheng Q, Tu J, Zhou W, He J, Zhong J, Chen Y, Wang J, Cai R, Zuo Y, Wei B, Fan Q, Yang J, Wu Y, Yi J, Li D, Liu M, Wang C, Zhou A, et al. (2019) SENP1-Sirt3 signaling controls mitochondrial protein acetylation and metabolism. Mol Cell 75:823-834.e5.
Wen S, Li Y, Shen X, Wang Z, Zhang K, Zhang J, Mei X (2021) Protective effects of zinc on spinal cord injury. J Mol Neurosci 71:2433-2440.
Wu YT, Wu SB, Wei YH (2014) Roles of sirtuins in the regulation of antioxidant defense and bioenergetic function of mitochondria under oxidative stress. Free Radic Res 48:1070-1084.
Xie W, Zhou P, Sun Y, Meng X, Dai Z, Sun G, Sun X (2018) Protective effects and target network analysis of ginsenoside Rg1 in cerebral ischemia and reperfusion injury: a comprehensive overview of experimental studies. Cells 7:270.
Xie W, Wang X, Xiao T, Cao Y, Wu Y, Yang D, Zhang S (2021) Protective effects and network analysis of ginsenoside Rb1 against cerebral ischemia injury: a pharmacological review. Front Pharmacol 12:604811.
Yang Y, Li S, Huang H, Lv J, Chen S, Pires Dias AC, Li Y, Liu X, Wang Q (2020) Comparison of the protective effects of ginsenosides Rb1 and Rg1 on improving cognitive deficits in SAMP8 mice based on anti-neuroinflammation mechanism. Front Pharmacol 11:834.
Ye JT, Li FT, Huang SL, Xue JL, Aihaiti Y, Wu H, Liu RX, Cheng B (2019) Effects of ginsenoside Rb1 on spinal cord ischemia-reperfusion injury in rats. J Orthop Surg Res 14:259.
Zeng H, Chen JX (2019) Sirtuin 3, endothelial metabolic reprogramming, and heart failure with preserved ejection fraction. J Cardiovasc Pharmacol 74:315-323.
Zhai M, Li B, Duan W, Jing L, Zhang B, Zhang M, Yu L, Liu Z, Yu B, Ren K, Gao E, Yang Y, Liang H, Jin Z, Yu S (2017) Melatonin ameliorates myocardial ischemia reperfusion injury through SIRT3-dependent regulation of oxidative stress and apoptosis. J Pineal Res 63:e12419.
Zhang H, Chen X, Wang X, Liu Y, Sands CD, Tang M (2021a) Ginsenoside Rb1 attenuates lipopolysaccharide-induced neural damage in the brain of mice via regulating the dysfunction of microglia and astrocytes. J Integr Neurosci 20:813-823.
Zhang J, Xiang H, Liu J, Chen Y, He RR, Liu B (2020) Mitochondrial sirtuin 3: new emerging biological function and therapeutic target. Theranostics 10:8315-8342.
Zhang JH, Yang HZ, Su H, Song J, Bai Y, Deng L, Feng CP, Guo HX, Wang Y, Gao X, Gu Y, Zhen Z, Lu Y (2021b) Berberine and ginsenoside Rb1 ameliorate depression-like behavior in diabetic rats. Am J Chin Med 49:1195-1213.
Zhao J, Lu S, Yu H, Duan S, Zhao J (2018) Baicalin and ginsenoside Rb1 promote the proliferation and differentiation of neural stem cells in Alzheimer's disease model rats. Brain Res 1678:187-194.
Zheng J, Shi L, Liang F, Xu W, Li T, Gao L, Sun Z, Yu J, Zhang J (2018) Sirt3 ameliorates oxidative stress and mitochondrial dysfunction after intracerebral hemorrhage in diabetic rats. Front Neurosci 12:414.
Zhou K, Zheng Z, Li Y, Han W, Zhang J, Mao Y, Chen H, Zhang W, Liu M, Xie L, Zhang H, Xu H, Xiao J (2020) TFE3, a potential therapeutic target for spinal cord injury via augmenting autophagy flux and alleviating ER stress. Theranostics 10:9280-9302.

C-Editor: Zhao M; S-Editors: Yu J, Li CH; L-Editors: Crawford M, Song LP; T-Editor: Jia Y

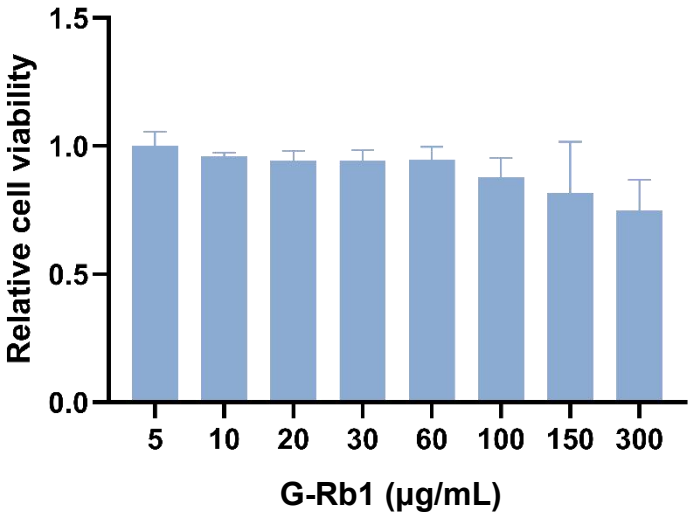

Additional Figure 1 Determination of G-Rb1 concentration *in vitro* using MTT.

The data (normalized by 5 μg/mL group) are mean ± SD (n = 3). The experiment was repeated three times. G-RB1: Ginsenoside Rb1; MTT: 3-(4,5-dimethylthiazol-2-yl)-2,5-diphenyltetrazolium bromide.